Nova scientia
ISSN: 2007-0705
Universidad de La Salle Bajío A. C., Coordinación de Investigación

Romero Toledo, Rafael; Ruíz Santoyo, Víctor;
Moncada Sánchez, Daniela; Martínez Rosales, Merced

Effect of aluminum precursor on physicochemical properties of Al2O3 by hydrolysis/precipitation method

Nova scientia, vol. 10, no. 20, 2018, pp. 83-99
Universidad de La Salle Bajío A. C., Coordinación de Investigación

DOI: 10.21640/ns.v10i20.1217

Available in: http://www.redalyc.org/articulo.oa?id=203358383006

Nova Scientia
Revista de Investigación de la Universidad De La Salle Bajío

Nº 20, Vol. 10 (1), 2018. **ISSN 2007 – 0705**, pp.: 83 - 99

Effect of aluminum precursor on physicochemical properties of Al_2O_3 by hydrolysis/precipitation method
Efecto del precursor de aluminio en las propiedades fisicoquímicas de la γ-Al_2O_3 por el método hidrólisis/precipitación

Rafael Romero Toledo[1], Víctor Ruíz Santoyo[2], Daniela Moncada Sánchez[3] y Merced Martínez Rosales[1]

Palabras clave: mesoporosos; hidrólisis-precipitación; oxi-hidróxido de aluminio; Al_2O_3
Keywords: mesoporous; hydrolysis/precipitation; low cost; Al_2O_3

Recepción: 27-10-2017 / Aceptación: 18-12-2017

Resumen

Este estudio reporta la síntesis de alúmina nano-fibrilar mesoporosa preparada por vía de hidrólisis-precipitación. Se realizó a partir de una solución acuosa de reactivo analítico (AR) de sulfato de aluminio y se comparó con un sulfato de aluminio grado técnico (TG) de baja pureza bajo condiciones similares usando amoníaco como agente precipitante. Las propiedades fisicoquímicas de estas muestras se estudiaron mediante diversas técnicas de caracterización, como el análisis térmico termogravimétrico y diferencial (TG/DTGA-DTA), difracción de rayos-X (DRX), Isotermas de adsorción-desorción N_2, Espectroscopía infrarroja (FTIR), tamaño de partícula y Microscopia Electrónica de Transmisión con análisis de Energía Dispersiva de rayos-X (TEM/EDAX). Los resultados de TG-DTA y XRD muestran una mayor estabilidad y una cristalinidad ligeramente mayor en la muestra de Al_2O_3-TG que Al_2O_3-AR. Los resultados de adsorción-desorción de N_2 muestran que ambos materiales tienen una alta área superficial de 311 m^2/g para Al_2O_3-TG y 272 m^2/g para Al_2O_3-AR exhibiendo características de materiales mesoporosos. Los resultados FTIR muestran un bajo porcentaje de grupos OH superficiales para Al_2O_3-TG, mostrando una acidez menor debido a la baja concentración de especies Al-OH (Al^{IV}). Las mediciones de TEM confirmaron que el tamaño de las fibras varió de 20 a 100 nm para Al_2O_3-TG y 20-80 nm para Al_2O_3-AR. El análisis EDAX muestra la presencia de 0.33% peso de Mg como impureza en Al_2O_3-TG. Se atribuye que esta cantidad es suficiente para generar defectos estructurales y disminuir ligeramente la acidez. Además, extendió la cadena fibrilar de la alúmina de Al_2O_3-TG.

[1]Universidad de Guanajuato, División de Ciencias Naturales y Exactas, Campus Guanajuato. E-mail: r.romerotoledo@ugto.mx
[2]Universidad de Guadalajara, Centro Universitario de los Altos
[3]Universidad de Guanajuato, Departamento de Ingeniería en Minas, Metalurgia y Geología

Abstract

This study reports the synthesis of mesoporous nano-fibrillar alumina prepared by hydrolysis-precipitation route. It was done from aqueous solution of aluminum sulfate analytical reagent (AR) and compared to aluminum sulfate technical grade (TG) of low purity under similar conditions using ammonia as the precipitating agent. The phisicochemical properties of these samples were studied with the assistance of characterization techniques such as Thermogravimetric and differential thermal analysis (TG/DTGA–DTA), X-ray diffraction (XRD), N_2 adsorption-desorption isotherms, Fourier transform infrared (FTIR) spectroscopy, particles size and Transmission electron microscopy with energy-dispersive X-ray analysis (TEM/EDAX). The TG-DTA and XRD results show greater stability and a slightly greater crystallinity in Al_2O_3-TG sample than Al_2O_3-AR. N_2 adsorption-desorption results show for both materials greatly surface area of 311 m^2/g for Al_2O_3-TG and 272 m^2/g for Al_2O_3-AR exhibiting characteristics of mesoporous materials. The FTIR results show a low percentage of surface OH groups for Al_2O_3-TG showing a lower acidity due to the low concentration of Al-OH species (Al^{IV}). TEM measurements confirmed that fibers size ranged from 20 to 100 nm, for Al_2O_3-TG and 20-80 nm, and for Al_2O_3-AR. EDAX shows the presence of 0.33 % wt. of Mg as an impurity in Al_2O_3-TG. It is attributed that this amount is sufficient to generate structural defects and decrease acidity slightly. Likewise, it extended the fibrillar chain of the alumina.

Introducción

Alumina is one of the most widely used materials as support in heterogeneous catalysis, adsorbent, electronic, abrasives, reinforcement of ceramic composites for its high strength, corrosion resistance, low thermal conductivity, and good electrical insulation due to several attractive features (Glorias *et al*., 2014; Yang, 2011, Jiratova *et al*., 1986). It is inexpensive and available in many different qualities making it suitable in a wide range of different chemical reactions. Furthermore, its synthesis is simple and economic. Though mainly used as support, alumina has also some catalytic activities by its own, this due to its acidity (Ancheyta *et al*., 2005). For specific applications, the surface area, the pore size, pore volume, thermal and mechanical stability of the support it has a large impact on the catalytic effect. Several Authors have emphasized that γ-Al_2O_3 with high pore volume may improve the adsorption performance if used as an adsorbent, and loading capacity if applied as a catalyst support, to minimize diffusion and transport influences (Xu

et al., 2016, Stanislaus *et al*., 2002). The alumina is a material that still stands in limelight owing to its extensive application.

The used aluminum oxides exist in a variety of metastable structures which are usually called transitions alumina such as η, χ, κ, θ, λ, δ and γ, as well as the stable α-Al_2O_3 phase. Especially, the variety of γ-alumina is widely appreciated due to its excellent properties as surface chemical properties that can be either acidic or basic depending on the transition alumina structure and the degree of hydration and hydroxylation of the surface, which is a major attraction from catalytic/adsorption point of view (Sinfontes *et al*., 2014; Zhang *et al*., 2016).

Nowadays, there are many materials as aluminum sources to synthesis and obtain Al_2O_3, for example $Al(NO_3)_3$, $Al_2(SO_4)_3$, $NH_4Al(SO_4)_2$, $AlCl_3$, $NaAlO_2$, amoung others. The mesoporous γ-Al_2O_3 synthesized with the above aluminum sources has excellent properties (Zhang *et al*., 2016). However, these aluminum sources are expensive, because of that; it is difficult to realize the industrialization with these ways. However, aluminum sulfate with the presence of impurities can be attractive, because of its low cost. The presence of impurities can influence in alumina quality and consequently affect the oxide morphology and/or physicochemical properties. Interestingly, even a tiny amount of impurities in the Al_2O_3 structure, can exert a strong effect on acidity, including structural defects. On other hand, a small amount of impurity could be detrimental for the performance. However, not all impurities are harmful; there are impurities that may present advantages benefiting the reaction and/or application. Among the impurities contained in alumina powders we can find: Na, Si, Fe, Ca, Mg, etc. Moreover, depending upon the synthesis method, alumina can contain anion impurities from the precursors used in the synthesis as for xample Cl^- ions, NO^{3-} or $(SO4)^{2-}$, something which is accepted by most of the people working in the field (Mishra *et al*., 2002).

Herein, we describe the synthesis and comparison of physic-chemicals features through several characterization techniques of two alumina materials prepared in similar conditions. One of them synthetized from an aqueous solution of aluminum sulfate analytical grade (Al_2O_3-AR) and a second alumina synthetized from aluminum sulfate technical grade with presence of impurities (Al_2O_3-TG), both alumina obtained by hydrolysis-precipitation route. We obtained materials with relatively high surface areas, with pore sizes and high pore volumes. Emphasis was put on the impurities of aluminum precursor and on the physic-chemical properties of the Al_2O_3. This paper contributes to a basic understanding of the purity of the aluminum salt and how it

influences on textural characteristics of mesoporous materials with the presence of 0.33 % wt. of Mg. This fundamental knowledge could be exploited in the design of new materials.

Materials and Method

Materials

In the present study, the starting materials to obtain hydrated alumina (Al_2O_3) were $Al_2(SO_4)_3$•$18H_2O$ with a purity of 95% (by weight, wt.) technical grade (TG), Alfa-Omega chemical, S. A. and an $Al_2(SO_4)_3$•$18H_2O$ with a purity of 99.98% (wt.), analytical reagent (AR), CTR Scientific, S.A., deionized water (Karal S. A.) and anhydrous NH_3 gas (Praxair, 99.98% (wt.)) as precipitant. Then, the impurities of both materials of aluminum sulfate are described (Table 1).

Table 1. Chemical composition wt. % by atomic adsorption of $Al_2(SO_4)_3$-TG, Alfa omega, S.A., and $Al_2(SO_4)_3$-AR, CTR Scientific, aluminium precursors.

Precursor	unsolvable	chlorides	Calcium	Magnesium	Potassium	Sodium	heavy metals	Iron
$Al_2(SO_4)_3$ TG	4±0.5%	ND	ND	0.33	ND	0.03	ND	0.03
$Al_2(SO_4)_3$ AR	0.003	<0.001	<0.0002	<0.0001	0.0002	<0.0075	<0.001	0.002%

**ND: Not Determined

Synthesis of pseudoboehmite

The flow chart of the preparation procedure is depicted in Figure 1. $Al_2(SO_4)_3$•$18H_2O$ TG and/or AR were dissolved into deionized water. The $Al_2(SO_4)_3$•$18H_2O$ technical grade was filtered for removal of insoluble impurities. Precursors were prepared by dropping saturated solution of aluminum sulfate into a solution of water and ammonia gas under rigorous magnetic stirring at temperature of 50-70 ºC. The precipitated solution was filtered; the precipitated of pseudoboehmite was rinsed with distilled water three times respectively, and then dried at 110 °C for 12 h. The phase change of pseudoboehmite to γ-Al_2O_3 was performed by thermal treatment at 500 °C for 7 h. The materials were labeled as follows: $Al_2(SO_4)_3$•$18H_2O$ Technical Grade (Al_2O_3-TG) and $Al_2(SO_4)_3$•$18H_2O$ Analytical Reagent (Al_2O_3-AR).

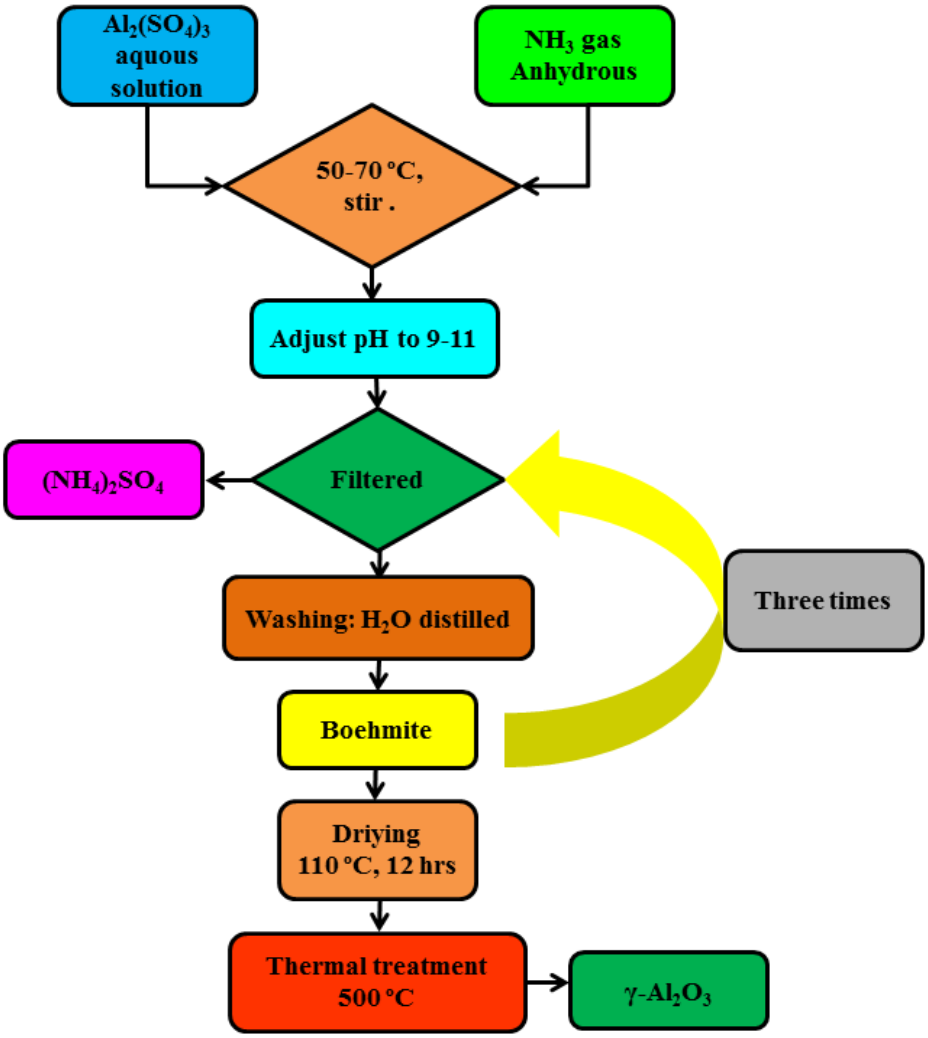

Figure 1. Flow chart of the preparation procedure of γ-Al_2O_3.

Materials characterization

Thermal analysis TGA-DTA

The thermal stability of the samples was carried by Thermogravimetric and Differential thermal analysis (TGA/DTGA-DTA) was performed from 30 ºC to 1000 °C in a Thermogravimetric analyzer SDT Q600 V20.5 Build 15 under air flow (100 mL / min) at a heating rate of 10 ºC/min.

N_2 physisorption

The textural properties were determined by N_2 adsorption (Micromeritics, ASAP 2010). The samples were degassed at 200 ºC for 3 h under vacuum. Nitrogen adsorption isotherms were measured at liquid N_2 temperature (77 K) and N_2 pressures ranging from 10^{-6} to 1.0 P/P_0. Surface

area was calculated according to Brunauer–Emmett–Teller (BET) method and the pore size distribution was obtained according to the Barret–Joyner–Halenda (BJH) method.

X-ray diffraction (XRD)

The crystalline properties of the samples were determined at room temperature by using X-ray powder diffraction. A siemens D-500 diffractometer equipped with a Cu Kα radiation anode was used for these measurements under the following conditions: sweep of 10-80º at an angle 2θ, with applied voltage of 30 kV and current of 20 mA.

FT-IR analysis

The vibrational spectroscopy measurements were performed at room temperature by Fourier transform infrared (FTIR) spectroscopy on a Bruker Model 27 spectrometer through KBr (99%) disk method in a frequency range of 4000 - 400 cm^{-1}.

Transmission electron microscopy (TEM/EDAX)

The morphology was studied by transmission electron microscopy (TEM) using a Philips Tecnai F20 microscope operating with a 200 kV equipped with energy dispersive X-ray spectroscopy (EDAX) for the determination of the chemical composition.

Particle size

The particle size of the materials was measured by electroacoustic, the technique with a particle size analyzer (AcoustoSizer II, ESA; Colloidal Dynamics, USA) to pH neutral.

Results and discussion

TEM/energy-dispersive X-ray (EDAX) analysis

The surface morphology of Al_2O_3-TG and Al_2O_3-AR samples is studied by TEM and the corresponding micrographs are presented in Figure 2. It can be seen that the products obtained represent typical TEM images of Al_2O_3 powders. They exhibit disordered morphology nanofibrillar with a length of about 20-100 nm for the Al_2O_3-TG and 20-80 nm for Al_2O_3-AR. The products obtained in our experiment are similar as those reported in the literature (Zhang *et al*., 2016). The development tendency of alumina is to be a more thermodynamically favored crystal

(Nuru *et al*., 2015; Yu *et al*., 2012). TEM images indicate alumina products have better dispersion performance for Al_2O_3-TG, which indicate alumina product obtained has good tendency to be a thermodynamic favored crystal due to presence of the Mg as impurity. Figure 2(c-d) shows the secondary particles size of the obtained products. The size varied from 0.45 μm to 0.85 μm for Al_2O_3-TG and from 0.35 μm to 0.65 μm for Al_2O_3-AR, observing a larger size for the sample Al_2O_3-TG, this is attributed to larger sizes of fibers that tend to form agglomerates or higher particles.

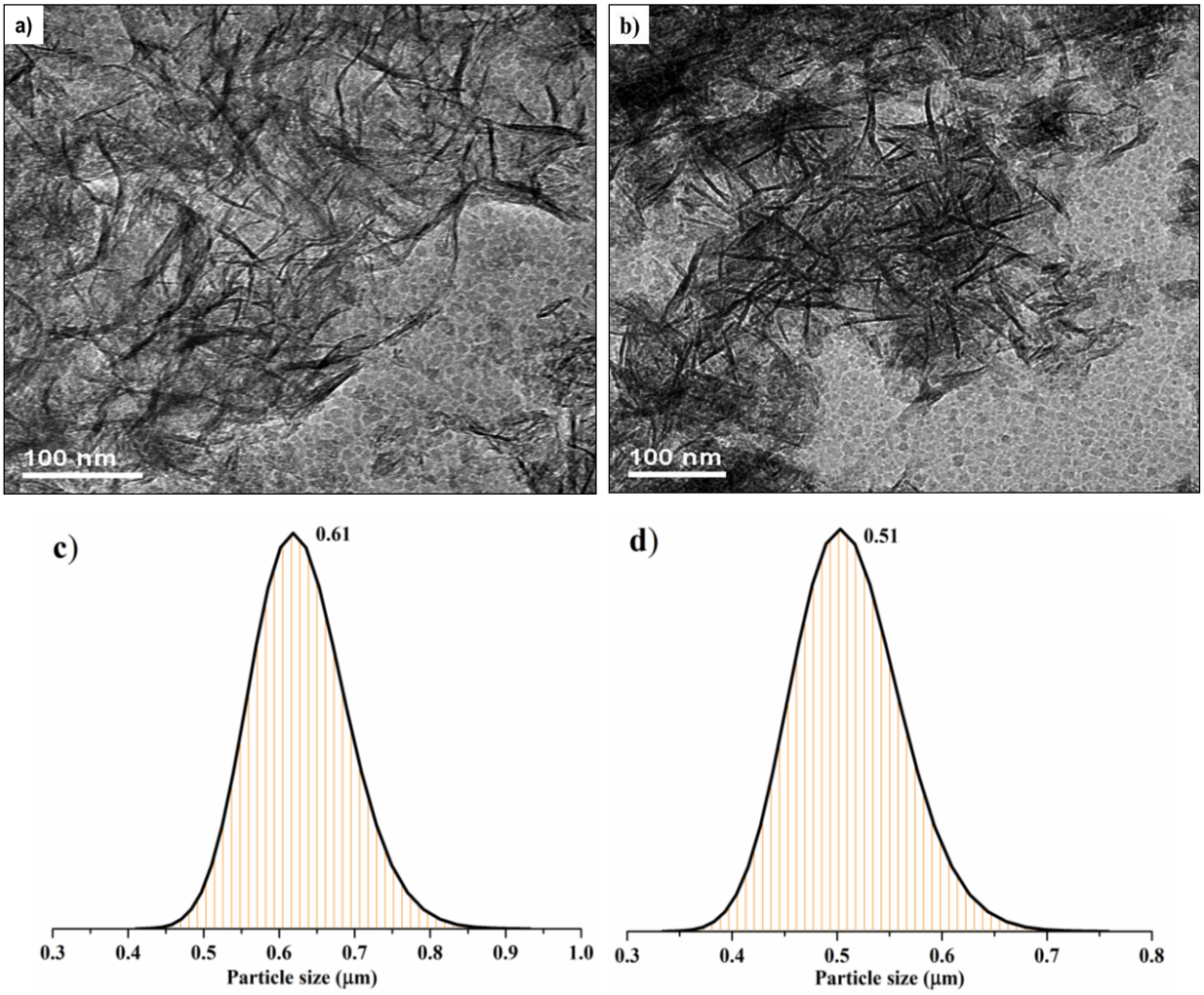

Figure 2. TEM images of a) Al_2O_3-TG, b) Al_2O_3-AR and particles size c) Al_2O_3-TG, d) Al_2O_3-AR

Energy dispersive X-ray **(**EDAX) data of both samples are provided in Table 2. The punctual analysis (EDAX) shows Al and O were detected on surfaces, respectively. The determination of

other present chemical elements as N and S are attributed to residues generated during the synthesis process. While than the presence of Mg is attributed as an impurity present in the low purity aluminum sulfate. The Mg was only possible to be observed since a micro-area analysis was performed. However, the assumption in this paper is that the trace element is homogenously distributed on the matrix and the limit is expressed as an atomic fraction, this attributing that the Na and Fe were removed during the synthesis process.

Table 2. Average elemental analysis of Al_2O_3-TG and Al_2O_3-AR.

	Elements: Atomic % by EDAX						
Sample	**O K**	**Al K**	**C K**	**Mg K**	**N K**	**S K**	**Total**
Al_2O_3-TG	57.96	15.58	24.28	0.20	2.84	0.07	100
Al2O3-AR	47.46	37.68	14.76	-	-	0.09	100

*(-): No detected

Thermogravimetric and differential thermal (TGA/DTGA–DTA) analysis

TGA/DTGA and DTA analysis of Al_2O_3-TG and Al_2O_3-AR are shown in Figure 3. Two endothermic peaks are observed in the DTA curve at 85 and 500 °C, the position of which varies with the type of the purity of aluminum salts that was used. The first peak is assigned to elimination of adsorbed water. At 500 °C pseudoboehmite decomposition to the γ-phase is produced; this involves dehydroxylation/dehydration $\left[2AlO(OH) \rightarrow \gamma\text{-}Al_2O_3 + H_2O\right]$. The derivative of thermogravimetric analysis DTGA and DTA shows a peak centred at 85 ºC indicating a thermal decomposition for Al_2O_3-TG. The weak broad DTGA and sharp DTA peaks around 500 ºC imply a transformation phase. These facts are confirmed by the thermogravimetric study, which shows a complete weight loss (17%) at 500 °C, this is consistent with the reported in the literature (Urretavizcaya *et al*., 1998). The Al_2O_3-AR shows two endothermic peaks, which are observed in the DTA curve at 60 and 500 °C. The first peak is assigned to elimination of adsorbed water. At 500 °C pseudoboehmite decomposition to the γ phase is produced. These facts are confirmed by the thermogravimetric study, which shows a complete weight loss (15%) at 500 °C.

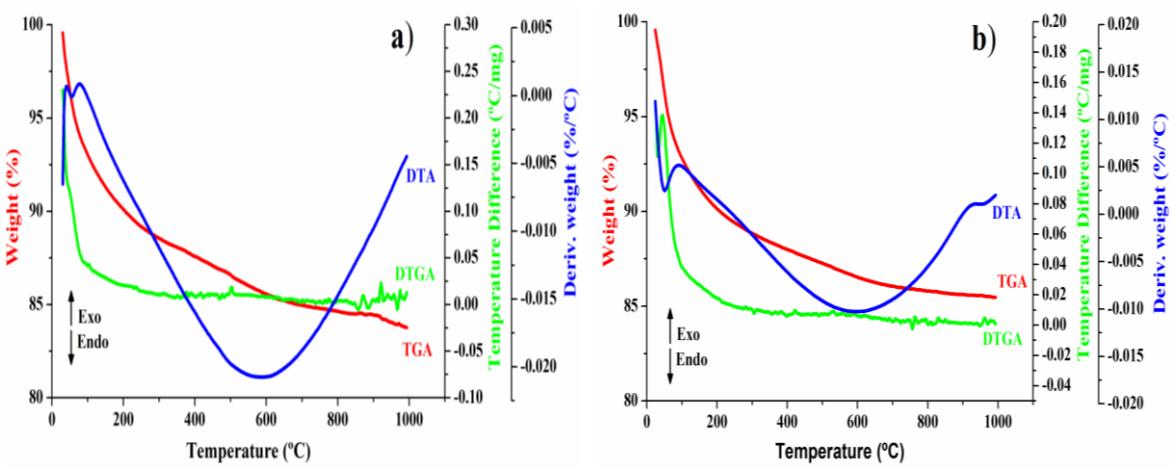

Figure 3. TGA/DTGA and DTA curves of a) Al_2O_3-TG and b) Al_2O_3-AR.

The endothermic peak observed in the DTA curve at 950 °C, Figure 3b, which is not accompanied by a weight loss (TGA), which is corroborated by DTGA, is attributed to θ-Al_2O_3 formation according to the reported in the literature (Jan *et al.*, 2014). Thermal transformations $\gamma\text{-}Al_2O_3 \rightarrow \delta\text{-}Al_2O_3 \rightarrow \theta\text{-}Al_2O_3 \rightarrow \alpha\text{-}Al_2O_3$ are not detected by DTA or TGA. In these transformations a small amount of energy is involved and no weight loss is produced. The temperature of phase transition is directly proportional to the grain size of the precursor. However, it is observed that Al_2O_3-TG exhibits greater thermal stability attributed to the presence of Mg. In fact several authors demonstrated that the presence MgO plays a structural role in the Al_2O_3 that altere its nature (Chen *et al.*, 2016).

Powder X-ray diffraction (XRD)

The high-angle XRD patterns of Al_2O_3-TG and Al_2O_3-AR samples are shown in figure 4. The X-ray diffraction pattern was performed of 10 – 80º at an angle 2θ. The results of the XRD patterns wide angle shows seven weak diffraction peaks, those are observed at 2θ= 19.2, 31.0, 36.6, 39.3, 46, 61.5, and 67º, which can be indexed as the (111), (220), (311), (222), (400), (511), and (440) reflections of γ-alumina according to JCPDS card: 100425 (Cheng *et al.*, 2006; Jan *et al.*, 2014). When the precursors are calcined at 500 ºC, there are no obvious peaks of others phases in XRD pattern indicating that the products structure is amorphous.

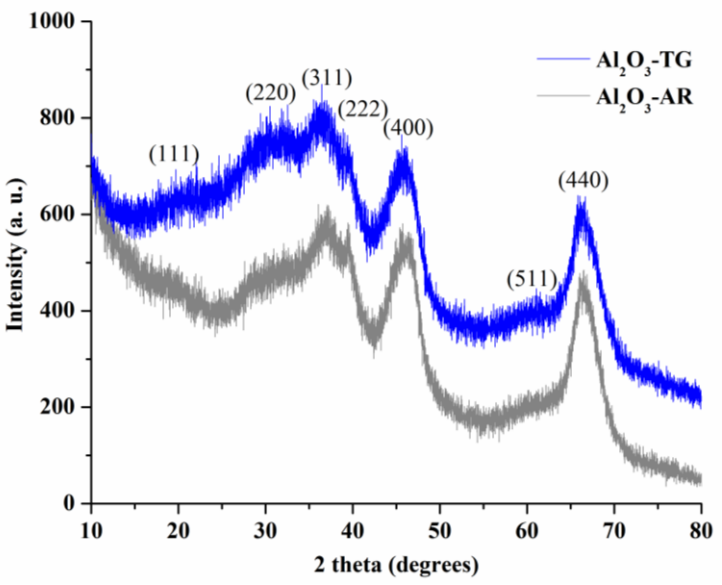

Figure 4. XRD patterns of a) Al_2O_3-TG and b) Al_2O_3-AR.

On other hand, a disorder in the structure can be observed. This disorder is reflected in the unusual broadening of some X-ray diffraction peaks for the Al_2O_3-TG material in the region 2θ=20-48°. This is attributed to a strong faulting on the (111), (110), and (100) in the spinel-like structure of these materials, which occur as individual and/or interconnected defects on different plane families (Sakashita *et al*., 2001). According to the literature, this non spinel model is more stable than spinel type structures (Wolverton *et al*., 2000). The XRD results confirm the TG-DTA analyses indicating that the Al_2O_3-TG is more stable that Al_2O_3-AR. However, in this work the structural defect is attributed to the presence of Mg. This is due to that excess alumina introduced a substitution defect on the tetrahedral magnesium site and an aluminum vacancy or magnesium vacancy is formed to compensate the positive charge excess, as reported in the literature (Yuji *et al*., 2006).

Adsorption/desorption analysis

The nitrogen adsorption isotherms and BJH pore size distribution of samples calcined at 500 ºC are shown in Figure 5. It is seen that the two materials exhibit the shape of type-IV Isotherm curves according to the IUPAC classification (Sing *et al*., 1985; Jan *et al*., 2014), which is characteristic of mesoporous materials. These materials show irregular shape isotherms with hysteresis loop type E and indicate that the pores in the material have an inkwell-type shape. Existence of the hysteresis loops is ascribed to the capillary condensation of N_2 gas occurring in the pores (Zhang *et al*., 2016).

Characterizations of powders obtained at 500 ºC and values reported in the literature by different authors from different routes of synthesis were shown in Table 3. Surface area and pore volume values of the materials were higher for the sample Al_2O_3-TG that for Al_2O_3-AR. Due to that exhibit nanofiber with a higher length, as it is shown in TEM images, it is attributed to the presence of Mg in the structure of the Al_2O_3-TG. A predominance of mesopores that could be of interest for heterogenous catalysis and the adsorption area is observed. In adittion, the intercrossing degree and disorder among the fibers (interfibrillar porosity) as well as their length may cause the non-uniform pore size distributions.

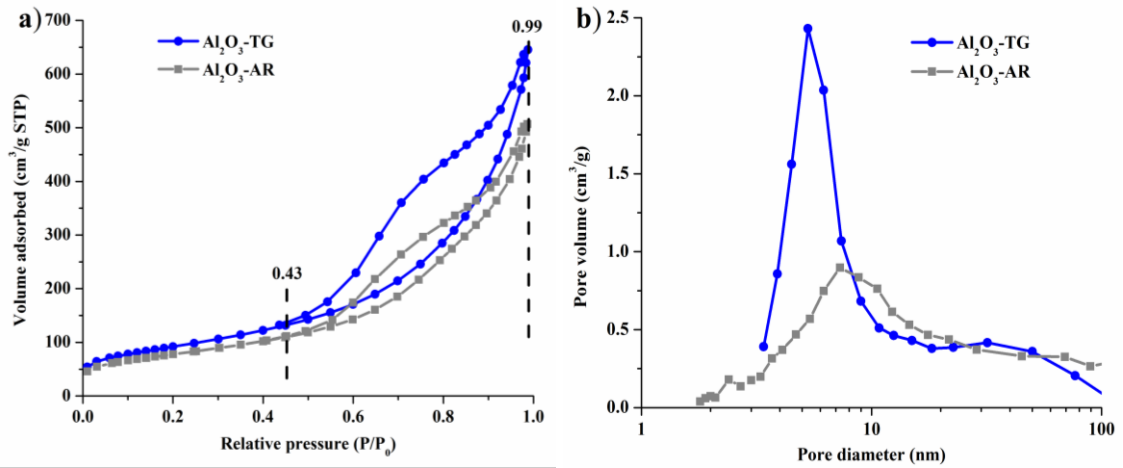

Figure 5. a) N_2 adsorption–desorption isotherm and b) pore size distribution curve of Al_2O_3-TG and Al_2O_3-AR.

Table 3. Results of the properties textural of samples obtained and reported by different synthesis routes.

Samples	**SSA[a]**	**Vap[b]**	**Dap[c]**	**References**
γ-Al_2O_3-TG (Hydrolysis-precipitation)	311	0.86	11.6	This work
γ-Al_2O_3-AR (Hydrolysis-precipitation)	272	0.76	10.8	This work
γ-Al_2O_3 (hydrolysis method)	183	0.4	10	Sifontes *et al*., 2014
γ-Al_2O_3 (hydrothermal route)	248	0.30	4.3	Guzman *et al*., 2005
γ-Al_2O_3 (CONDEA commercial)	220	-	5.9	Del Angel *et al*., 2005
γ-Al_2O_3 (Template method)	328.9	0.81	12.0	Renuka *et al*., 2016
γ-Al_2O_3 (precipitation/digestión)	220	0.48	7.0	Potdar *et al*., 2007
γ-Al_2O_3 (dual-templating route)	320	0.60	7.0	Sandeep *et al*., 2015
Mesoporuos Alumina (double hydrolysis method)	335.5	0.60	7.1	Benjing *et al*., 2017
γ-Al_2O_3 (sol–gel method)	370	0.52	6.0	Rudina *et al*., 2012

γ-Al_2O_3 (sol-gel hydrolysis method)	236	0.4	7.0	Wei *et al*., 2016
γ-Al_2O_3 commercial (J&K chemical)	331	-	5.8	Zongbo *et al*., 2016
γ-Al_2O_3 (Solid state Method)	220	0.49	6.1	Soodeh *et al*., 2016
γ-Al_2O_3 (coprecipitation method)	346.4	1.0	10.2	Zhang *et al*., 2016
γ-Al_2O_3 (Reverse precipitation method)	240	0.90	7.6	Wu *et al*., 2012
γ-Al_2O_3 (coprecipitation/sol-gel method)	264	0.30	5.1	Mohammed *et al*., 2012

[a] Specific surface area (m^2/g)
[b] Average pore volume (cm^3/g)
[c] Average pore diameter (nm)

The comparative values obtained and reported by different authors from several synthetic pathways are similar and in some cases higher. This textural behavior is typical of materials where condensation occurs mainly between particles. This is related to grain size. After the calcination there is a considerable increase in the values of specific areas caused by dehy-droxylation leading to the formation of γ-Al_2O_3. It is seen that the synthesized material from an inexpensive aluminum precursor with impurity presence make larger nanofibers presenting very attractive textural properties obtained by a simple and economical synthesis method.

Fourier transforms infrared spectroscopy (FT-IR) analysis

The FTIR spectra for the different products obtained, is shown in Figure 6. The results of the sinthesized materials are consistent with the reported in literature (Riad *et al*., 2007). In the FT-IR patterns, the broad band at 3200–3700 cm^{-1} its characteristic of -OH stretching vibration that is bonded to Al^{3+}, and the band at 1638 cm^{-1} corresponding to physisorbed water are observed. Meanwhile the peak at 1470 cm^{-1} was also due to water deformation vibrations (Boumaza *et al*., 2009). Band appearing at 1100 cm^{-1} is typically for γ-alumina due to Al–O vibration mode (Xu *et al*., 2017). The valley between 1000 cm^{-1} and 435 cm^{-1} confirms the γ-form, and the one at 873 cm^{-1} is assigned to the bending vibrations of Al-O bond. Al-O-Al bond in the gamma phase of alumina generates the band at 670 cm^{-1} (Cheng *et al*., 2006). These results are consistent with the XRD analysis where the g-phase was identified.

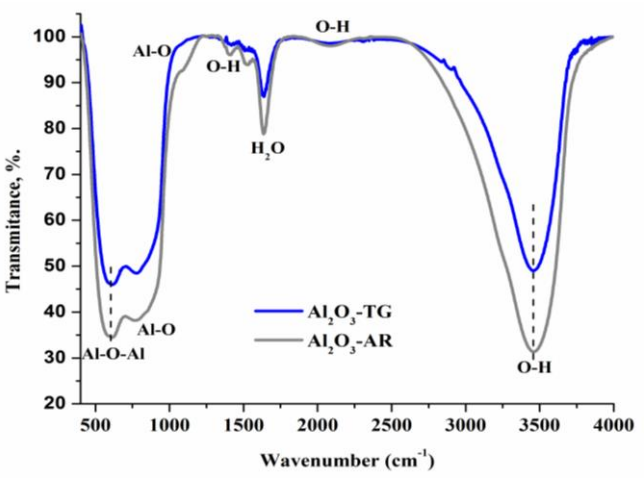

Figure 6. FT-IR spectra of Al_2O_3-TG and Al_2O_3-AR.

The peaks in the region of 500 – 750 cm^{-1} are assigned to Al^{VI}, whereas the shoulder at 750 and the line at 890 cm^{-1} are assigned to Al^{IV}. Thus, γ-Al_2O_3 phase contains both tetrahedral and octahedral coordination (Renuka *et al*., 2012). In this sense, it is possible to observe more intense vibrations and slightly more widened in the material Al_2O_3-AR, reason why a greater content of the tetrahedral coordination assuming a greater acidity is attributed. Several Authors have observed that the presence of Mg decreases the weak Brønsted acidity and increases the basicity of the alumina (Zhang *et al*., 2016). Then that product obtained of Al_2O_3-TG presents lower content of tetrahedral coordination.

Effect of salt's purity

The results clearly show that the presence of Mg into the Al crystal lattice change the acid and basic properties of this oxide. It is interesting to verify that the values of the surface area (Table 3) change when comparing Al_2O_3-TG with Al_2O_3-AR. In recent years the use of different grades of aluminum salts have become important areas of research and development due to their importance as precursors for aluminum oxides. In some applications, such as advanced manufacturing alumina-based ceramics, and high-purity aluminium oxides compounds are required. Here tolerable concentrations of impurities are rather low and an analytical control became a limiting step of the technology (Koksal *et al*., 2002). Other applications that required high-purity aluminum oxides are pharmaceuticals products, refractories, electronics, among others (Mishra, 2002). However, there are applications where the presence of impurities can benefits the application or reaction, as

mentioned earlier. This study determined that a small amount of impurity in precursor salt can modify the physical properties of alumina compared with conventional γ-alumina. In addition it, exhibit attractive properties for several applications as the process of adsorption and catalytic, in addition to a low cost.

Conclusion

The material of γ-Al_2O_3 nanofibrillar synthesized by hydrolysis-precipitation method presented physicochemical properties attract as possible catalytic support and adsorbent material. The results showed that 0.33 wt. % of Mg as impurity was sufficient to generate structural defects and decreased the acidity in the Al_2O_3-TG material. However, the presence of Mg extended the fibrillar chain of the alumina besides giving greater thermal stability and greater textural properties. Hence from precursors of aluminum with presence of impurities can be obtained attractive materials for several applications.

Acknowledgements

Authors gratefully acknowledge the support by the National Council on Science and Technology (CONACyT) and University of Guanajuato, México.

Referencias

Ancheyta, J., Rana, M. S., & Furimsky, E. (2005). Hydroprocessing of heavy petroleum feeds: Tutorial. Catalysis Today, 109(1), 3-15.

Antony Stanislaus, Khalida Al-Dolama, Mamun Absi-Halabi. (2002). Preparation of a large pore alumina-based HDM catalyst by hydrothermal treatment and studies on pore enlargement mechanism. Journal of Molecular Catalysis A: Chemical 181, 33–39.

Benjing Xu, Yang Yang, Yanyan Xu, Baozhai Han, Youhe Wang, Xinmei Liu, Zifeng Yan. (2017). Synthesis and characterization of mesoporous Si-modified alumina with high thermal stability. Microporous and Mesoporous Materials 238, 84-89.

Boumaza, A., Favaro, L., Lédion, J., Sattonnay, G., Brubach, J. B., Berthet, P., & Tétot, R. (2009). Transition alumina phases induced by heat treatment of boehmite: an X-ray diffraction and infrared spectroscopy study. Journal of solid state chemistry, 182(5), 1171-1176.

D. Mishra, S. Anand, R.K. Panda, R.P. Das. (2002). Effect of anions during hydrothermal preparation of boehmites. Materials Letters 53. 133–137.

G. Del Angel, C. Guzma´n, A. Bonilla, G. Torres, J.M. Padilla. (2005). Lanthanum effect on the textural and structural properties of γ-Al_2O_3 obtained from Boehmite. Materials Letters 59, 499– 502.

Glorias-Garcia, F., Arriaga-Merced, J. M., Roa-Morales, G., Varela-Guerrero, V., Barrera-Díaz, C. E., & Bilyeu, B. (2014). Fast reduction of Cr (VI) from aqueous solutions using alumina. Journal of Industrial and Engineering Chemistry, 20(4), 2477-2483.

H.S. Potdar, Ki-Won Jun, Jong Wook Bae, Seung-Moon Kim, Yun-Jo Lee. (2007). Synthesis of nano-sized porous γ-alumina powder via a precipitation/digestion route. Applied Catalysis A: General 321, 109–116.

Jan Barta, Milan Pospisil, Vaclav Cuba. (2014). Indirect synthesis of Al_2O_3 via radiation- or photochemical formation of its hydrated precursors. Materials Research Bulletin 49, 633–639.

Jing Xu, Abdul-Rauf Ibrahim, Xiaohui Hu, Yanzhen Hong, Yuzhong Su, Hongtao Wang, Jun Li. (2016). Preparation of large pore volume γ-alumina and its performance as catalyst support in phenol hydroxylation. Microporous and Mesoporous Materials. 231, 1-8.

Jiri Koksal, Vaclav Synek, Pavel Janos. (2002). Extraction-spectrometric determination of lead in high-purity aluminium salts. Talanta 58, 325 – 330.

Jun-Cheng, L., Lan, X., Feng, X., Zhan-Wen, W., & Fei, W. (2006). Effect of hydrothermal treatment on the acidity distribution of γ-Al_2O_3 support. Applied Surface Science, 253(2), 766-770.

K. Jiratova, M. Kraus. (1986). Effect of support properties on the catalytic activity of HDS catalysts. Applied Catalysis, 27, 21–29.

M.L. Guzman-Castillo, F. Hernandez Beltran, J.J. Fripiat, A. Rodriquez Hernandez, R. Garcıa de Leon, J. Navarrete Bolanos, A. Tobon Cervantes, X. Bokhimi. (2005). Physicochemical properties of aluminas obtained from different aluminum salts. Catalysis Today 107–108.

Mohammed A. Al-Daous, Abdullah A. Manda, Hideshi Hattori. (2012). Acid–base properties of γ-Al_2O_3 and MgO–Al_2O_3 supported gold nanoparticles. Journal of Molecular Catalysis A: Chemical 363– 364, 512– 520.

Pratima Mishra. (2002). Low-temperature synthesis of α-alumina from aluminum salt and urea. Materials Letters 55, 425–429.

Qi Yang. (2011). Synthesis of γ-Al_2O_3 nanowires through a boehmite precursor route. Bulletin of Materials Science. Vol. 34, pp. 239–244.

Renuka, N. K., Shijina, A. V., & Praveen, A. K. (2012). Mesoporous γ-alumina nanoparticles: synthesis, characterization and dye removal efficiency. Materials letters, 82, 42-44.

Riad, M. (2007). Influence of magnesium and chromium oxides on the physicochemical properties of γ-alumina. Applied Catalysis A: General, 327(1), 13-21.

Rudina Bleta, Pierre Alphonse, Lisa Pin, Marie Gressier, Marie-Joëlle Menu. (2012). An efficient route to aqueous phase synthesis of nanocrystalline c-Al2O3 with high porosity: From stable boehmite colloids to large pore mesoporous alumina. Journal of Colloid and Interface Science 367, 120–128.

Sakashita, Y., Araki, Y., & Shimada, H. (2001). Effects of surface orientation of alumina supports on the catalytic functionality of molybdenum sulfide catalysts. Applied Catalysis A: General, 215(1), 101-110.

Sandeep Badoga, Rajesh V. Sharma, Ajay K. Dalai, John Adjaye. (2015). Synthesis and characterization of mesoporous aluminas with differentpore sizes: Application in NiMo supported catalyst for hydrotreatingof heavy gas oil. Applied Catalysis A: General 489, 86–97.

Sifontes, Á. B., Gutiérrez, B., Mónaco, A., Yanez, A., Díaz, Y., Méndez, F. J., & Brito, J. L. (2014). Preparation of functionalized porous nano-γ-Al_2O_3 powders employing colophony extract. Biotechnology Reports, 4, 21-29.

Sing, K. S. (1985). Reporting physisorption data for gas/solid systems with special reference to the determination of surface area and porosity (Recommendations 1984). Pure and applied chemistry, 57(4), 603-619.

Soodeh Sepehri, Mehran Rezaei, Gabriella Garbarino, Guido Busca. (2016). Facile synthesis of a mesoporous alumina and its application as a support of Ni-based autothermal reforming catalysts. International journal of hydrogen energy 41, 3456-3464.

Urretavizcaya, G., Cavalieri, A. L., Lopez, J. P., Sobrados, I., & Sanz, J. (1998). Thermal evolution of alumina prepared by the sol-gel technique. Journal of Materials Synthesis and Processing, 6(1), 1-7.

Wei Wu, Zhijian Wan, Mingming Zhu, Dongke Zhang. (2016). A facile route to aqueous phase synthesis of mesoporous alumina with controllable structural properties. Microporous and Mesoporous Materials 223, 203-212.

Wenbin Chen, Hong Nie, Dadong Li, Xiangyun Long, Jacob van Gestel, Francoise Maugé. (2016). Effect of Mg addition on the structure and performance of sulfide Mo/Al_2O_3 in HDS and HDN reaction. Journal of Catalysis 344 (2016) 420–433.

Wenzhan Yu, BinYang, Xiumin Chen, Wenlong Jiang, Qingchun Yu, Baoqiang Xu. (2012). Thermodynamic calculation and experimental investigation on the products of carbothermal reduction of Al_2O_3 under vacuum. Vacuum. P. 2005-2009.

Wolverton, C., & Hass, K. C. (2000). Phase stability and structure of spinel-based transition aluminas. Physical Review B, 63(2), 024102.

Xu, B., Yang, Y., Xu, Y., Han, B., Wang, Y., Liu, X., & Yan, Z. (2017). Synthesis and characterization of mesoporous Si-modified alumina with high thermal stability. Microporous and Mesoporous Materials, 238, 84-89.

Y. S. Wu, J. Ma, F. Hu and M. C. Li. (2012). Synthesis and Characterization of Mesoporous Alumina via a Reverse Precipitation Method. J. Mater. Sci. Technol., 28(6), 572–576.

Yuji Okuyama, Noriaki Kurita, Norihiko Fukatsu. (2006). Defect structure of alumina-rich nonstoichiometric magnesium aluminate spinel. Solid State Ionics 177 (2006) 59 – 64.

Z.Y.Nuru, L.Kotsedi, C.J.Arendse, D.Motaung, B.Mwakikunga, K.Roro, M.Maaza. (2015). Thermal stability of multilayered $Pt\text{-}Al_2O_3$ nanocoatings for high temperature CSP systems. Vacuum. P. 115-120.

Zhang, L., Wu, Y., Zhang, L., Wang, Y., & Li, M. (2016). Synthesis and characterization of mesoporous alumina with high specific area via co-precipitation method. Vacuum, 133, 1-6.

Zhang, L., Wu, Y., Zhang, L., Wang, Y., & Li, M. (2016). Synthesis and characterization of mesoporous alumina with high specific area via co-precipitation method. Vacuum, 133, 1-6.

Zongbo Shi, Wenqian Jiao, Li Chen, Peng Wu, Yimeng Wang, Mingyuan He. (2016). Clean synthesis of hierarchically structured boehmite and γ-alumina with a flower-like morphology. Microporous and Mesoporous Materials 224, 253-261.